Journal of Reproduction and Development, Vol. 62, No 2, 2016

—Original Article—

Ultrastructural comparison of porcine putative embryonic stem cells derived by *in vitro* fertilization and somatic cell nuclear transfer

Hyunju YOO[1)], Eunhye KIM[1)], Seon-Ung HWANG[1)], Junchul David YOON[1)], Yubyeol JEON[1)], Kyu-Mi PARK[1)], Kyu-Jun KIM[1)], Minghui JIN[1)], Chang-Kyu LEE[2)], Eunsong LEE[3)], Hyunggee KIM[4)], Gonhyung KIM[1)] and Sang-Hwan HYUN[1)]

[1)]*Laboratory of Veterinary Embryology and Biotechnology (VETEMBIO), College of Veterinary Medicine, Chungbuk National University, Cheongju 28644, Republic of Korea*

[2)]*Department of Agricultural Biotechnology, Animal Biotechnology Major, and Research Institute for Agriculture and Life Science, Seoul National University, Seoul 08826, Republic of Korea*

[3)]*Laboratory of Theriogenology, College of Veterinary Medicine, Kangwon National University, Kangwon 24341, Republic of Korea*

[4)]*Department of Biotechnology, School of Life Sciences and Biotechnology, Korea University, Seoul 02841, Republic of Korea*

Abstract. The ultrastructure of porcine putative embryonic stem cells and porcine fetal fibroblasts (PFFs) was analyzed by transmission electron microscopy. The aim of this study was to compare the features of organelles in *in vitro* fertilization (IVF) derived porcine embryonic stem cells (IVF-pESCs) and somatic cell nuclear transfer (SCNT) derived pESCs (SCNT-pESCs). Also, the features of organelles in high-passage IVF-pESCs were compared with those in low-passage cells. The ultrastructure of PFFs showed rare microvilli on the cell surfaces, polygonal or irregular nuclei with one to two reticular-shaped nucleoli and euchromatin, low cytoplasm-to-nucleus ratios, rare ribosomes, rare rough endoplasmic reticulum, elongated mitochondria, rich lysosomes and rich phagocytic vacuoles. IVF-pESCs showed rare microvilli on the cell surfaces, round or irregular nuclei with one to two reticular-shaped nucleoli and euchromatin, low cytoplasm-to-nucleus ratios, rich ribosomes, long stacks of rough endoplasmic reticulum, elongated mitochondria, rare lysosomes and rare autophagic vacuoles. By contrast, SCNT-pESCs showed rich microvilli with various lengths and frequencies on the cell surfaces, polygonal nuclei with one reticular shaped nucleoli and heterochromatin, high cytoplasm-to-nucleus ratios, rare ribosomes, rare rough endoplasmic reticulum, round mitochondria, rich lysosomes and rich phagocytic vacuoles with clear intercellular junctions. Furthermore, high-passage IVF-pESCs showed irregularly shaped colonies, pyknosis and numerous lysosomes associated with autophagic vacuoles showing signs of apoptosis. In conclusion, this study confirms that the ultrastructural characteristics of pESCs differ depending on their origin. These ultrastructural characteristics might be useful in biomedical research using pESCs, leading to new insights regarding regenerative medicine and tissue repair.

Key words: Embryonic stem cell, Porcine, Transmission electron microscopy, Ultrastructure

(**J. Reprod. Dev. 62:** 177–185, 2016)

Embryonic stem cells (ESCs) are derived from the inner cell mass (ICM) of blastocyst-stage embryos [1–3]. ICM cells are isolated by immunosurgery and cultured on mitomycin C-inactivated mouse embryonic fibroblasts (MEFs) as feeder layers [1, 2]. ESCs are undifferentiated cells that have the capacity for unlimited proliferation and can differentiate into various types of cell or tissue *in vivo* and *in vitro* [2, 4, 5]. Pigs are a useful and meaningful model in many branches of medicine because they are immunologically and physiologically similar to humans [6–8]. It is believed that porcine ESCs (pESCs) can play important roles in biomedical research as models for cell therapy, regenerative medicine and tissue repair in humans [8–10]. For these reasons, the establishment of a pESC line has become very important. Consequently, many researchers have attempted to establish porcine ES, ES-like or ICM cell lines by using preimplantation blastocysts [9, 11, 12]. Furthermore, several authors have reported establishment of pESCs from preimplantation blastocysts derived by *in vitro* fertilization (IVF) and somatic cell nuclear transfer (SCNT) [13–15]. pESCs can proliferate stably in an undifferentiated state *in vitro* with MEFs as feeder layers and basic fibroblast growth factor (bFGF) [14–17].

Some of the characteristics of pESCs, including their pluripotency-related molecular markers, karyotype and signaling pathways, have been reported [14, 18]. However, details of the ultrastructure of pESCs have not been reported previously. Transmission electron microscopy (TEM) is a major analysis method in cell biology [19, 20] and a useful method in cancer research, virology and ESC research [21–24]. TEM techniques can provide useful information about the

Received: September 2, 2015
Accepted: December 15, 2015
Published online in J-STAGE: January 28, 2016

Correspondence: S-H Hyun (e-mail: shhyun@cbu.ac.kr) and G Kim (e-mail: ghkim@cbu.ac.kr)

functionality of cells. The ultrastructural characteristics of mouse ESCs (mESCs) [25], nonhuman primate ESCs [1] and human ESCs (hESCs) [26], as well as embryoid bodies (EBs) derived from mESC lines [27, 28], have been reported. Moreover, Talbot *et al.* reported the ultrastructure of porcine blastocysts [29]. Porcine blastocysts had nuclei, Golgi complexes, numerous mitochondria, free ribosomes and polysomes, very large lipid droplets, microfilaments, microtubules and junctional complexes with tight junctions and desmosomes [29].

Most of the above ultrastructural features were documented by TEM. However, TEM images of the ultrastructure of pESCs derived by IVF and SCNT have not been reported previously. We analyzed the ultrastructure of porcine fetal fibroblasts (PFFs) and pESCs derived by IVF and SCNT by TEM. The aim of this study was to compare the features of organelles in IVF-pESCs and SCNT-pESCs. Since it was required to understand the apoptosis of pESCs during long-term culture *in vitro*, we also compared the features of organelles in high-passage IVF-pESCs with those in low-passage IVF-pESCs.

Materials and Methods

Ethics statement

This study was carried out in strict accordance with the recommendations in the Guide for the Care and Use of Laboratory Animals of the National Veterinary and Quarantine Service. The protocol was approved by the Committee on the Ethics of Animal Experiments of Chungbuk National University (Permit Number: CBNUA-584-13-01). All animals were sacrificed under isoflurane anesthesia, and all efforts were made to minimize suffering.

Chemicals

Unless otherwise indicated, all chemicals and reagents used in the present study were purchased from Sigma-Aldrich (St. Louis, MO, USA).

Preparation of the feeder cell layer

The MEFs used as the feeder cell layer were prepared from ICR mice. ICR mice were killed at pregnancy day 13 and fetuses were recovered. Fetal heads, internal organs and legs were removed. The remaining tissues were minced in fresh phosphate-buffered saline (PBS) and centrifuged at 2000 rpm for 3 min at least twice until MEFs were obtained. MEFs were cultured in Dulbecco's modified Eagle's medium (DMEM, Gibco, Carlsbad, CA, USA) containing 10% FBS (Gibco), 1% non-essential amino acids (Gibco), 1% glutamine (Gibco), 0.1 mM β-mercaptoethanol (Gibco) and 1% antibiotics-antimycotics (Gibco) (growth medium) at 37ºC under 5% CO_2 in air. MEFs were passaged two to three times before inactivation with mitomycin C (10 μg/Ml, Roche, Basel, Switzerland) for 2–2.5 h for use in culture of pig blastocysts. Inactivated MEFs were plated at a density of 5×10^5 cells/ml in a four-well dish coated with 0.5% gelatin and containing growth medium. The MEFs were usually plated 1 day before seeding of porcine embryos or ICMs.

Cell culture

All of the pESC lines were established and characterized in a previous study [30]. In brief, hatched porcine blastocysts were obtained by IVF and SCNT using *in vitro* matured (IVM) oocytes. Oocyte collection and maturation, sperm preparation, donor cell preparation, IVF and SCNT were performed as previously reported [31–33]. The blastocysts were collected 7 days after IVF and SCNT. The growth medium of inactive feeder cells was replaced with pESC culture medium 2 h before blastocyst plating. The pESC culture medium consisted of low-glucose DMEM/F10 (Gibco) containing 1% non-essential amino acids, 1% glutamine, 0.1 mM β-mercaptoethanol, 1% antibiotics-antimycotics, 4 ng/ml bFGF (Invitrogen, Carlsbad, CA, USA) and 15% FBS. Blastocysts were removed from the zona pellucida using 0.5% protease. For plating, blastocysts were washed three times in pESC culture medium. They were then seeded on a monolayer of mitomycin C-inactivated MEFs in four-well plates (Nunc, Roskilde, Denmark). The plating efficiency of primary cultures was determined by scoring the number of attached colonies after 48 h. The timing of the disaggregation of primary colonies was based on morphology and size. The medium was replaced daily, and new colonies were subcultured at an interval of approximately 7–10 days, according to their size and growth rate. PFFs were isolated according methods in a previous report [34] and cultured in DMEM (Gibco) containing 10% FBS (Gibco), 1% non-essential amino acids (Gibco), 1% glutamine (Gibco), 0.1 mM β-mercaptoethanol (Gibco) and 1% antibiotics-antimycotics (Gibco) (growth medium) at 37ºC under 5% CO_2 in air. The attachment and growth of PFFs were examined daily, and the culture medium was replaced every 2 days. The cells were at passage 2. pESC lines derived by IVF and SCNT were grown in monolayer culture on mitomycin C-treated MEFs. Seven-day-old colonies were individually peeled off the feeder layer with glass capillaries and dissected using two syringe needles. The pESC medium, including bFGF, was replaced every day. pESC culture was performed in medium at 37ºC under 5% CO_2 in a humidified atmosphere.

Transmission electron microscopy

For TEM analysis, two lines of pESCs derived from IVF blastocysts (IVF0227_P20 and IVF0214_P37) and one line of pESCs derived from SCNT blastocysts (Transgenic pESC_P20) line were prepared. The donor cells used for SCNT were transgenic cell lines overexpressing the 11beta hydroxysteroid dehydrogenase (11β-HSD1) gene. All of the pESCs were grown on a feeder layer in four-well plates. Subsequently, pESCs were peeled off the feeder layer and collected into tubes. Furthermore, PFFs were trypsinized and collected into tubes. The cells were washed with 0.1 M phosphate buffer (pH 7.2) twice for 5 min, and cell pellets were resuspended directly in 2.5% glutaraldehyde fixative (EMS, Fort Washington, PA, USA) in 0.1 M phosphate buffer (pH 7.2) and stored at 4ºC overnight. Then, the cells were washed in 0.1 M phosphate buffer (pH 7.2) for 5 min three times. After washing, the cells were transferred to 1% osmium tetroxide (OsO_4) (EMS) in 0.1 M phosphate buffer (pH 7.2) for 1 h and then washed for 10 min three times in the same buffer. Additionally, the cells were washed twice in distilled water for 5 min each. The fixed cells were dehydrated in an ascending series of ethanol solutions (Merck, Rahway, NJ, USA) (50%, 60%, 70%, 80%, 90%, 95% and 100%; 15 min each), and washed three times in 100% ethanol for 15 min each. The cells were then washed twice in 100% propylene oxide (EMS) for 30 min each and embedded in Epon 812 (EMS). The cells were infiltrated with propylene oxide:Epon 812 (3:1) for

3 h followed by propylene oxide:Epon 812 (1:1) overnight. Next, the cells were infiltrated with propylene oxide:Epon 812 (1:3) for 3 h and then 100% Epon 812 for 3 h. Subsequently the resin was polymerized in an oven at 70ºC for 12 h. Semithin sections were cut with a glass knife (EMS), all sections were prepared using an ultramicrotome (Ultracut UCT, Leica), and ultrathin sections were cut with a diamond knife (DiATOME, Hatfield, PA, USA). Semithin sections were stained with toluidine blue (EMS). Ultrathin sections were first contrasted with 2% uranyl acetate (EMS) for 10 min, rinsed with double-distilled water, contrasted with lead citrate (EMS) for 1 min and rinsed with distilled water. Finally, the contrasted ultrathin sections were examined and photographed under a transmission electron microscope (JEM-1400Plus, JEOL, Tokyo, Japan).

Results

Ultrastructural analysis of colony shape and microvilli

As shown in Table 1 and Fig. 1, the cell surface showed various shapes of colonies and microvilli depending on the type of cell line. PFFs and SCNT-pESCs, as observed by TEM, grew as round or polygonal colonies (Fig. 1A and 1D). By contrast, IVF-pESCs grew as irregularly shaped colonies (Fig. 1B). Furthermore, the microvilli had various lengths and frequencies (Fig. 1A, 1B and 1D). SCNT-pESCs had numerous microvilli (Fig. 1D). By contrast, microvilli occurred rarely on PFFs and IVF-pESCs (Fig. 1A and 1B).

Ultrastructural analysis of the nucleus

We analyzed the ultrastructure of the nucleus, nucleolus, nuclear envelope and chromatin in all of the cell lines (Table 2 and Fig. 2). The nuclei in PFFs had a polygonal or irregular shape and contained one or two dense nucleoli (Fig. 2A and 2B). The nuclei in IVF-pESCs were deeply infolded and of round or irregular shape (Fig. 2C). Moreover, they had one to two prominent nucleoli that were reticular shaped and dark (Fig. 2C). The nuclei in SCNT-pESCs were large and polygonal, and the one nucleolus was reticular shaped (Fig. 2D). As shown in Fig. 2, all cell lines had a nuclear envelope. Moreover, the chromatin in the PFFs and IVF-pESCs was observed as low-density, electron-lucent nuclear material (Fig. 2A, 2B and 2C). Euchromatin occupied most of the nuclear space. Conversely, SCNT-pESCs had heterogeneous structures containing euchromatin and heterochromatin (Fig. 2D). The cytoplasm-to-nucleus ratio was low in PFFs and IVF-pESCs (Fig. 2A, 2B and 2C) and high in SCNT-pESCs (Fig. 2D).

Ultrastructural analysis of protein-synthesis-associated organelles

The important function of ribosomes, the rough endoplasmic reticulum (rER) and the Golgi apparatus (Table 3 and Fig. 3) is protein synthesis. As shown in TEM micrographs, the rER was rarely observed in PFFs and SCNT-pESCs (Fig. 3A and 3D). Furthermore, the cytoplasm of these cells contained few free ribosomes and polysomes. By contrast, long stacks of ribosome-studded rER were observed in IVF-pESCs (Fig. 3B and 3C). The rER was often extensive and rich in free ribosomes/polysomes. On the other hand, the Golgi apparatus was rarely observed in the cytoplasm in all cell lines.

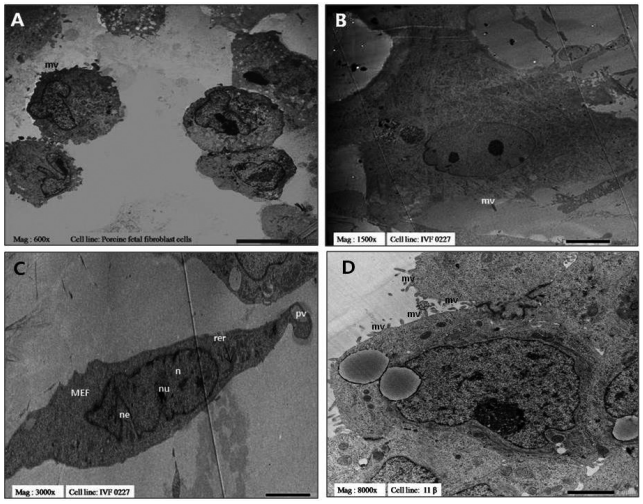

Fig. 1. Transmission electron micrographs of the cell surface. (A) Porcine fetal fibroblasts, magnification × 600. (B) *In vitro* fertilization-derived IVF 0227 pESCs, magnification × 1500. (C) pESC lines co-cultured with mouse embryonic fibroblasts (MEFs), magnification × 3000. n, nucleus; nu, nucleolus; ne, nuclear envelope; pv, phagocytic vacuole; rer, rough endoplasmic reticulum. (D) Transgenic pESCs derived by SCNT, magnification × 8000. mv, microvilli.

Table 1. Ultrastructural comparison of colonies and microvilli in three cell lines

Origin	Cell line	Organelle	
		Cell surface	
		Colonies	Microvilli
PFFs	Fetal fibroblasts	Round or polygonal	Rare
IVF	IVF0227	Irregular	Rare
SCNT	Transgenic pESCs	Round or polygon	Rich

PFFs, porcine fetal fibroblasts; IVF, *in vitro* fertilization; SCNT, somatic cell nuclear transfer.

Ultrastructural analysis of intracellular digestion-associated organelles

Intracellular digestion-associated organelles include phagocytic vacuoles, autophagic vacuoles and lysosomes (Table 4 and Fig. 4). Round phagocytic vacuoles containing membranous structures were frequently seen in PFFs and SCNT-pESCs, but not in IVF-pESCs. Autophagic vacuoles containing dense irregular bodies were also observed, although they were not seen in PFFs and SCNT-pESCs and were rare in IVF-pESCs. In addition, lysosomes were frequently seen in PFFs and SCNT-pESCs as round electron-dense cytoplasmic structures (Fig. 4A, 4B and 4D). By contrast, lysosomes were not prominent in IVF-pESCs (Fig. 4C).

Ultrastructural analysis of mitochondria

Mitochondria with different shapes and sizes were observed in all cell lines (Table 5 and Fig. 5). Elongated well-developed mitochondria were observed frequently in PFFs (Fig. 5A and 5B). Furthermore,

Table 2. Ultrastructural comparison of the nucleus in three cell lines

Origin	Cell line	Organelle				
		Nucleus				
		Nucleus	Nucleolus	Nuclear envelope	Chromatin	C:N ratio
PFFs	Fetal fibroblasts	Polygonal or irregular	One to two	Normal	Euchromatin	Low
IVF	IVF0227	Round or irregular	One to two	Normal	Euchromatin	Low
SCNT	Transgenic pESCs	Polygonal	One	Normal	Heterogeneous	High

PFFs, porcine fetal fibroblasts; IVF, *in vitro* fertilization; SCNT, somatic cell nuclear transfer; C, cytoplasm; N, nucleus.

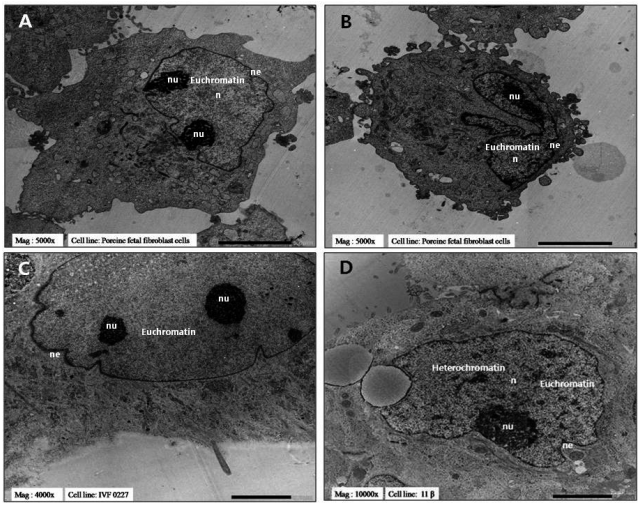

Fig. 2. Transmission electron micrographs of the nucleus. (A, B) Porcine fetal fibroblasts, magnification × 5000. (C) *In vitro* fertilization-derived IVF 0227 pESCs, magnification × 4000. (D) Transgenic pESCs derived by SCNT, magnification × 10000. n, nucleus; nu, nucleolus; ne, nuclear envelope.

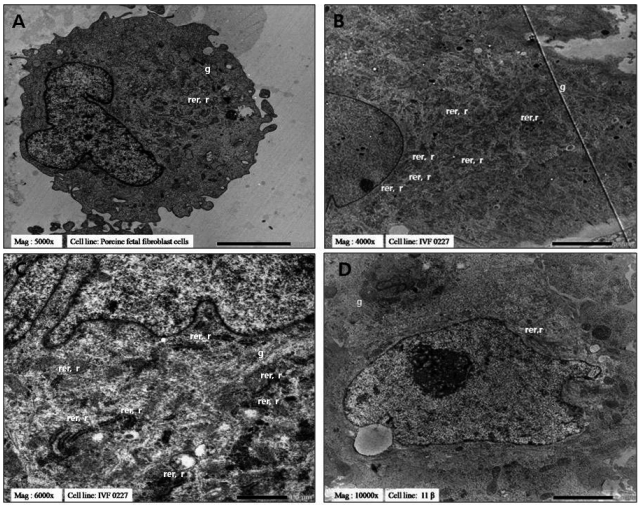

Fig. 3. Transmission electron micrographs of protein-synthesis-associated organelles. (A) Porcine fetal fibroblasts, magnification × 5000. (B) *In vitro* fertilization-derived IVF 0227 pESCs, magnification × 4000. (C) *In vitro* fertilization-derived IVF 0227 pESCs, magnification × 6000. (D) Transgenic pESCs derived by SCNT, magnification × 10000. r, ribosome; rer, rough endoplasmic reticulum; g, Golgi apparatus.

the cristae of the PFFs mitochondria were distinct and arranged in parallel. Similarly, elongated well-developed mitochondria were seen in IVF-pESCs (Fig. 5C). However, the cristae of the mitochondria were not distinct. By contrast, round well-developed mitochondria were observed frequently in SCNT-pESCs (Fig. 5D). Moreover, the cristae of the SCNT-pESC mitochondria were distinct and arranged in parallel.

Ultrastructural analysis of intercellular junctions

Intercellular junctions including desmosome-like junctions and gap junctions were observed between adjacent cells, and the cells were closely apposed (Table 6 and Fig. 6). Intercellular junctions were seen in PFFs and SCNT-pESCs, but not in IVF-pESCs. Desmosome-like junctions and gap junctions were infrequently observed in PFFs. By contrast, these junctions were frequently seen in SCNT-pESCs.

Ultrastructural comparison of pESCs of various origins with mESCs and hESCs

This is the first ultrastructural comparison between pESC lines and ESCs from other species [25, 26] (Table 7). Ultrastructural examination showed that the colony morphology of PFFs and

Table 3. Ultrastructural comparison of the protein synthesis-associated organelle in three cell lines

Origin	Cell line	Organelle		
		Protein synthesis		
		Ribosomes	Rough ER	Golgi apparatus
PFFs	Fetal fibroblasts	Rare	Rare	Rare
IVF	IVF0227	Rich	Rich	Rare
SCNT	Transgenic pESCs	Rare	Rare	Rare

PFFs, porcine fetal fibroblasts; IVF, *in vitro* fertilization; SCNT, somatic cell nuclear transfer; ER, endoplasmic reticulum.

SCNT-pESCs was similar to that of mESCs [25]. In general, PFFs, SCNT-pESCs and mESCs were round, whereas IVF-pESCs had an irregular shape. Furthermore, the nuclei of PFFs and SCNT-pESCs were polygonal and resembled the nuclei of hESCs [26]; the nuclei of IVF-pESCs were similar to those of mESCs. PFFs, IVF-pESCs, mESCs and hESCs all showed euchromatin, whereas SCNT-pESCs

Table 4. Ultrastructural comparison of the intracellular digestion-associated organelle in three cell lines

Origin	Cell line	Organelle		
		Intracellular digestion		
		Phagocytic vacuole	Autophagic vacuole	Lysosome
PFFs	Fetal fibroblasts	Rich	Absent	Rich
IVF	IVF0227	Absent	Rare	Rare
SCNT	Transgenic pESCs	Rich	Absent	Rich

PFFs, porcine fetal fibroblasts; IVF, *in vitro* fertilization; SCNT, somatic cell nuclear transfer.

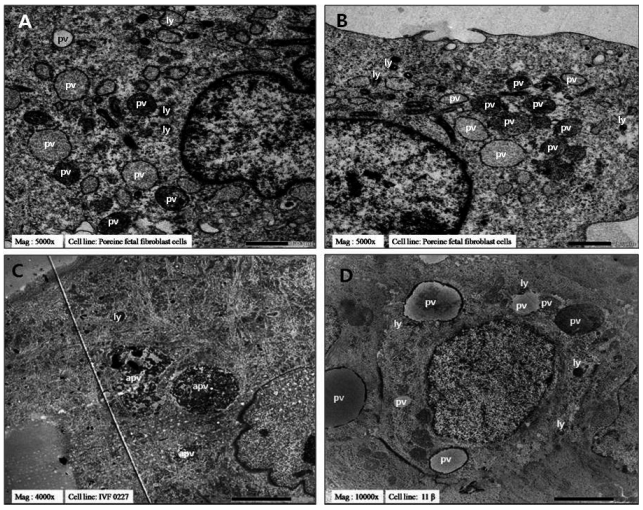

Fig. 4. Transmission electron micrographs of intracellular digestion-associated organelles. (A, B) Porcine fetal fibroblasts, magnification × 5000. (C) *In vitro* fertilization-derived IVF 0227 pESCs, magnification × 4000. (D) Transgenic pESCs derived by SCNT, magnification × 10000. pv, phagocytic vacuole; apv, autophagic vacuole; ly, lysosome.

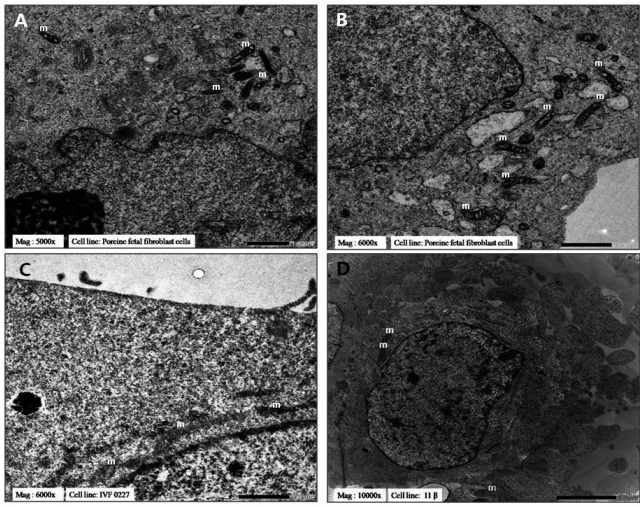

Fig. 5. Transmission electron micrographs of mitochondria. (A) Porcine fetal fibroblasts, magnification × 5000. (B) Porcine fetal fibroblasts, magnification × 6000. (C) *In vitro* fertilization-derived IVF 0227 pESCs, magnification × 6000. (D) Transgenic pESCs derived by SCNT, magnification × 10000. m, mitochondrion.

Table 5. Ultrastructural comparison of the mitochondrion in three cell lines

Origin	Cell line	Organelle	
		Mitochondrion	
		Development	Shape
PFFs	Fetal fibroblasts	Well	Elongated
IVF	IVF0227	Well	Elongated
SCNT	Transgenic pESCs	Well	Round

PFFs, porcine fetal fibroblasts; IVF, *in vitro* fertilization; SCNT, somatic cell nuclear transfer.

showed heterogeneous structures containing heterochromatin and euchromatin. Additionally, the cytoplasm-to-nucleus ratio was low in PFFs, IVF-pESCs and mESCs and high in SCNT-pESCs and hESCs. All mitochondria in PFFs, IVF-pESCs and hESCs were well developed and elongated. By contrast, well-developed round mitochondria were observed in SCNT-pESCs and mESCs.

Ultrastructural analysis of high-passage IVF-pESCs

As shown in Table 8 and Fig. 7, TEM examination showed that the organelles of high-passage IVF-pESCs (IVF0214) were different from those of low-passage IVF-pESCs (IVF0227). Pyknosis and wrinkled nuclear envelopes were evident in high-passage IVF-pESCs, but not in low-passage IVF-pESCs (Fig. 2C and 7A, 7C, 7F). Furthermore, the chromatin in low-passage IVF-pESCs was low-density euchromatin, whereas high-passage IVF-pESCs displayed heterogeneous structures containing heterochromatin and euchromatin (Fig. 2C and 7C). Additionally, autophagic vacuoles and lysosomes were frequently observed in high-passage IVF-pESCs but were infrequent in low-passage IVF-pESCs (Fig. 4C and 7D, 7F). TEM examination further showed that the organelles of high-passage IVF-pESCs were similar to those of differentiated hESCs (Table 9). The nuclei in high-passage IVF-pESCs and differentiated hESCs showed pyknosis and wrinkled nuclear envelopes (Fig. 7C). Moreover, high-passage IVF-pESCs and differentiated hESCs had a high chromatin density. Additionally, the rER and lysosomes were frequently observed in high-passage IVF-pESCs and differentiated hESCs (Fig. 7A and 7B).

Table 6. Ultrastructural comparison of intercellular junctions in three cell lines

Origin	Cell line	Organelle	
		Intercellular junctions	
		Desmosome-like	Gap
PFFs	Fetal fibroblasts	Rare	Rare
IVF	IVF0227	Absent	Absent
SCNT	Transgenic pESCs	Rich	Rich

PFFs, porcine fetal fibroblasts; IVF, *in vitro* fertilization; SCNT, somatic cell nuclear transfer.

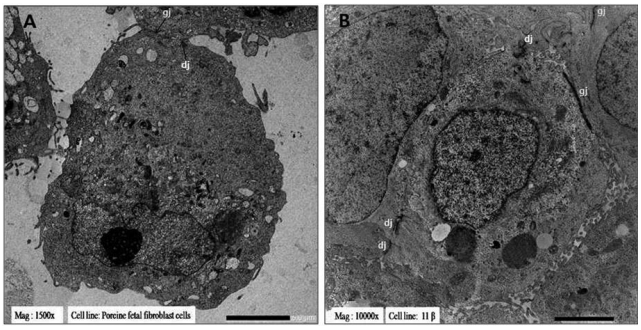

Fig. 6. Transmission electron micrographs of intercellular junctions. (A) Porcine fetal fibroblasts, magnification × 1500. (B) Transgenic pESCs derived by SCNT, magnification × 10000. gj, gap junction; dj, desmosome-like junction.

Table 7. Ultrastructural comparison of pESCs of various origins with mESCs and hESCs

Organelle	Origin			Other species of ESCs	
	PFFs	IVF	SCNT	Mouse (Baharvand *et al.* 2003)	Human (Sathananthan *et al.* 2002)
Colony	Round or polygonal	Irregular	Round or polygonal	Round	Saucer
Nucleus	Polygonal or irregular	Round or irregular	Polygonal	Round or irregular	Polygonal
Nucleolus	One to two	One to two	One	One to three	One to three
Chromatin	Euchromatin	Euchromatin	Heterogeneous	Euchromatin	Euchromatin
C:N ratio	Low	Low	High	Low	High
Mitochondrion	Elongated	Elongated	Round	Round	Elongated

PFFs, porcine fetal fibroblasts; IVF, *in vitro* fertilization; SCNT, somatic cell nuclear transfer; C, cytoplasm; N, nucleus.

Table 8. Ultrastructural comparison of low- and high-passage in pESCs derived by IVF

Organelle	Cell line	
	In vitro fertilization derived	
	IVF0227	IVF0214
	Low passage (20th)	High passage (37th)
Colony	Irregular	Irregular
Nucleus	Round or irregular	Pyknosis and irregular
Nuclear envelope	Normal	Wrinkle
Chromatin	Euchromatin	Heterogeneous
Autophagic vacuole	Rare	Rich
Lysosome	Rare	Rich
Mitochondrion	Elongated	Poor and elongated

Discussion

This study was the first to compare the ultrastructure of different pESC lines using TEM. We observed microvilli, nuclei containing reticulated nucleoli, rERs, Golgi apparatuses, lysosomes and mitochondria in the pESC lines derived from various origins. Compared with PFFs and IVF-pESCs, SCNT-pESCs had more microvilli on their surfaces, which suggests that they have high absorption and secretory activity, resulting in an increase in cell surface area. Microvilli indicate highly metabolic activity and have also been observed in mESCs, mouse EBs and hESCs [25–27].

Large or small deeply infolded euchromatin- or heterochromatin-containing nuclei with one to three reticular-shaped nucleoli and a nuclear envelope were generally seen in all pESC lines. These features indicate that the nucleus controls gene expression and mediates DNA replication during the cell cycle. The TEM appearance of the nucleus was similar to that reported in other hESCs and mESCs [25, 26]. Also, the nuclear shape and structure were similar to those in the blastocysts of many mammalian species [35–37]. Nucleoli were the prominent contrasted structures in the nuclei of all pESC lines observed by TEM. In most cells, the nucleus contained one or a few nucleoli. Reportedly, mammalian nuclei contain one or a few nucleoli, and the size and organization of the nucleoli are directly related to ribosome production [38, 39]. Furthermore, we observed heterochromatin in SCNT-pESCs and high-passage IVF-pESCs. This result indicates that the chromatin in SCNT-pESCs and high-passage IVF-pESCs is highly condensed and is typically not transcribed [40, 41]. In PFFs and IVF-pESCs, but not SCNT-pESCs, the nucleus-to-cytoplasm ratio was low, which may indicate high maturity of SCNT-pESCs.

In this study, the rER was seen to be in contact with ribosomes. Similar observations have been reported in mammalian embryos, blastocysts and cells [35, 37, 42, 43]. Also, the rER has been described in porcine blastocysts [29]. Additionally, the patterns of rER and

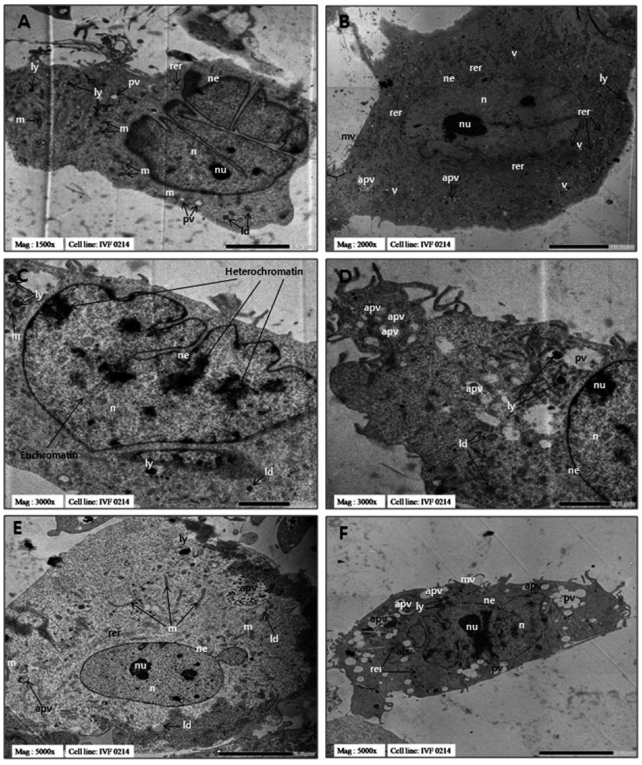

Fig. 7. Transmission electron micrographs of *in vitro* fertilization-derived IVF0214 pESCs (high passage and cultured *in vitro* after 37 passages). (A) Ultrastructure of a nucleus-associated organelle, magnification × 1500. (B) Ultrastructure of a protein-synthesis-associated organelle, magnification × 2000. (C) Ultrastructure of a nucleus-associated organelle, magnification × 3000. (D) Ultrastructure of an intracellular digestion-associated organelle, magnification × 3000. (E) Ultrastructure of a mitochondrion-associated organelle, magnification × 5000. (F) Ultrastructure of a nucleus-associated organelle, magnification × 5000. n, nucleus; nu, nucleolus; ne, nuclear envelope; m, mitochondrion; pv, phagocytic vacuole; apv, autophagic vacuole; ly, lysosome; v, vesicle; ld, lipid droplets; rer, rough endoplasmic reticulum; mv, microvilli.

ribosome frequency found here were similar to those reported in hESCs and mESCs [25, 26]. As shown in TEM micrographs, the rER is formed in all pESC lines by series of stacks arranged in parallel. On the other hand, the Golgi apparatus was rarely observed and had flattened cisternae in all pESC lines, possibly indicating low activity of this organelle. This low activity could lead to decreased protein secretion. This finding may reflect the protein quantities required by all pESC lines to proliferate. The Golgi apparatus is involved in protein synthesis and export of cellular products for secretion [44–46]. The Golgi apparatus has also been described in porcine epiblast cells [29].

Phagocytic vacuoles and lysosomes perform a central role in intracellular digestion. They were observed frequently in PFFs and SCNT-pESCs but were rare in IVF-pESCs. Phagocytic vacuoles and lysosomes were observed in the blastocysts of mammalian species [37, 47, 48] and in human and bovine embryos [43, 47]. The lysosome is a cellular organelle that contains acid hydrolases to degrade delivered materials. Digestion of phagocytic vacuoles by the enzymes contained within lysosomes releases their nutrients into the cytoplasm [49]. Evidence of phagocytosis was observed in PFFs and SCNT-pESCs. Phagocytosis is involved in the acquisition of nutrients by cells. Furthermore, it is critical for the uptake and degradation of infectious agents and senescent cells and contributes to development, tissue remodeling, the immune response and inflammation [50]. Autophagic vacuoles were not observed frequently in the cytoplasm of any pESC line. However, the presence of autophagic vacuoles in high-passage IVF-pESCs suggests that autophagy has roles in catabolism, degradation and production of amino acids under starvation conditions, recycling of cellular components, prevention of various diseases and cell death [51, 52]. These findings suggest that autophagy is an adaptive response to stress that promotes survival, whereas in other cases, it appears to promote cell morbidity.

In the present study, mitochondria in all pESC lines varied in size and shape and had mostly tubular cristae. Elongated and round mitochondria were detected in all pESC lines. The elongated mitochondria resembled those found in porcine blastocysts and hESCs [26, 29]. By contrast, round mitochondria are frequently found in mESCs [25]. Furthermore, we found that well-developed mitochondria were present at a high frequency in all three pESC lines. Previous reports demonstrated that adult bovine oocytes have

Table 9. Ultrastructural comparison of pESCs (IVF-high passage) with mESCs and hESCs

Organelle	Cell line	Other species		
	Porcine ESCs (IVF 0214)	Mouse ESCs (Baharvand *et al.*)	Human ESCs (Sathananthan *et al.*)	
	High passage	Undifferentiated	Undifferentiated	Differentiated
Colony	Irregular	Round	Saucer	Goblet
Nucleus	Pyknosis and irregular	Round or irregular	Polygonal	Pyknosis
Nuclear envelope	Wrinkle	Normal	Normal	Wrinkle
Chromatin density	High	Low	Low	High
Rough ER	Rich	Rich	Rare	Rich
Lysosome	Rich	Rare	Rare	Rich
Mitochondrion	Poor and elongated	Round	Elongated	Elongated

C, cytoplasm; N, nucleus; ER, endoplasmic reticulum.

a larger mitochondrial population compared with calf oocytes, suggesting that the adult bovine oocytes are mature [53]. Moreover, the mitochondria localization of striated ducts was also clear. PFFs and IVF-pESCs contain elongated mitochondria with a dense matrix, whereas SCNT-pESCs contain round mitochondria with a pale matrix. These findings suggest that the differences in mitochondrial structure among pESC lines were accompanied by a functional difference [54]. Furthermore, the presence of mitochondria is an indication of metabolic activity [55]. Also, several studies showed that mitochondria are involved in other processes, such as signaling, ATP production, energy metabolism, cellular differentiation and cell death, as well as control of the cell cycle and cell growth [54, 56, 57]. Mitochondrial cristae are folds of the mitochondrial inner membrane that provide an increase in surface area [56]. The study of mitochondrial function has become central to a wide variety of clinical and basic science research [58, 59].

Contact areas of similar appearance were observed in PFFs and SCNT-pESCs, in which they were often associated with gap junctions and desmosome-like junctions. These junctions are thought to hold cells together and facilitate communication between neighboring cells [60, 61]. Previous reports demonstrated gap junctions and desmosome-like junctions in many mammalian embryos and blastocysts [29, 35, 37, 42, 47, 62–64]. However, gap junctions and desmosome-like junctions were not observed in hESCs and mESCs [25, 26].

TEM analysis of high-passage IVF-pESCs revealed signs of apoptosis (Fig. 7). Apoptosis is a strictly regulated mechanism for the ordered removal of aged or damaged cells [65, 66]. In general, ultrastructural analyses of low-passage IVF-pESCs showed normal nuclei, few lysosomes, few autophagic vacuoles and elongated mitochondria. By contrast, high-passage IVF-pESCs had pyknosis, wrinkly nuclear envelopes, numerous lysosomes associated with autophagic vacuoles and poor mitochondria. Features of apoptosis include chromatin condensation, nuclear fragmentation, apoptotic bodies and lack of mitochondrial swelling [65–69]. Therefore, the high-passage IVF-pESCs showed the initial signs of apoptosis.

This study confirms that pESCs of different origins have a characteristic ultrastructure. We identified differences and similarities among the pESC lines. The results of this study show that the ultrastructural features of PFFs are similar to those of SCNT-pESCs, but not IVF-pESCs. This presumably indicates that the cells have different states. Furthermore, this study demonstrated that the features of organelles are origin dependent. Previous reports demonstrated the ultrastructure of porcine embryos and blastocysts [29, 37, 70, 71]. Also, TEM permits precise demonstration of the ultrastructure of various ESCs [25, 26]. However, the present study is the first report of the ultrastructure of pESCs.

In conclusion, this study confirmed that the ultrastructural characteristics of pESCs differ depending on their origin. The comparison of the different pESC lines provides useful information regarding the ultrastructure of pESCs. The ultrastructural characteristics might facilitate biomedical and histological research on pESCs. Also, the ultrastructure of pESCs could play an important role in cell therapy, regenerative medicine, tissue repair and use of pESCs as a human cell biology model.

Acknowledgments

This work was supported, in part, by the intramural research grant of Chungbuk National University in 2015, and a grant from the Cooperative Research Program for Agriculture Science & Technology Development (Project No. PJ011077, PJ011288), Rural Development Administration, and National Research Foundation of Korea Grants funded by the Korean Government (NRF-2013R1A2A2A04008751), Republic of Korea.

References

1. **Thomson JA, Marshall VS.** Primate embryonic stem cells. *Curr Top Dev Biol* 1998; **38**: 133–165. [Medline] [CrossRef]
2. **Thomson JA, Itskovitz-Eldor J, Shapiro SS, Waknitz MA, Swiergiel JJ, Marshall VS, Jones JM.** Embryonic stem cell lines derived from human blastocysts. *Science* 1998; **282**: 1145–1147. [Medline] [CrossRef]
3. **Takahashi K, Yamanaka S.** Induction of pluripotent stem cells from mouse embryonic and adult fibroblast cultures by defined factors. *Cell* 2006; **126**: 663–676. [Medline] [CrossRef]
4. **Friel R, van der Sar S, Mee PJ.** Embryonic stem cells: understanding their history, cell biology and signalling. *Adv Drug Deliv Rev* 2005; **57**: 1894–1903. [Medline] [CrossRef]
5. **Wobus AM.** Potential of embryonic stem cells. *Mol Aspects Med* 2001; **22**: 149–164. [Medline] [CrossRef]
6. **Kobayashi E, Hishikawa S, Teratani T, Lefor AT.** The pig as a model for translational research: overview of porcine animal models at jichi medical university. *Trans Res* 2012; **1**: 653–664.
7. **Luo Y, Lin L, Bolund L, Jensen TG, Sørensen CB.** Genetically modified pigs for biomedical research. *J Inherit Metab Dis* 2012; **35**: 695–713. [Medline] [CrossRef]
8. **Tumbleson ME.** Swine in biomedical research. *Source Mod Biomed Research* 2008; **2**: 233–239.
9. **Li M, Zhang D, Hou Y, Jiao L, Zheng X, Wang W-H.** Isolation and culture of embryonic stem cells from porcine blastocysts. *Mol Reprod Dev* 2003; **65**: 429–434. [Medline] [CrossRef]
10. **Hall V.** Porcine embryonic stem cells: a possible source for cell replacement therapy. *Stem Cell Rev* 2008; **4**: 275–282. [Medline] [CrossRef]
11. **Notarianni E, Galli C, Laurie S, Moor RM, Evans MJ.** Derivation of pluripotent, embryonic cell lines from the pig and sheep. *J Reprod Fertil Suppl* 1991; **43**: 255–260. [Medline]
12. **Wheeler MB.** Development and validation of swine embryonic stem cells: a review. *Reprod Fertil Dev* 1994; **6**: 563–568. [Medline] [CrossRef]
13. **Chen L-R, Shiue YL, Bertolini L, Medrano JF, BonDurant RH, Anderson GB.** Establishment of pluripotent cell lines from porcine preimplantation embryos. *Theriogenology* 1999; **52**: 195–212. [Medline] [CrossRef]
14. **Vackova I, Ungrova A, Lopes F.** Putative embryonic stem cell lines from pig embryos. *J Reprod Dev* 2007; **53**: 1137–1149. [Medline] [CrossRef]
15. **Kim HS, Son HY, Kim S, Lee GS, Park CH, Kang SK, Lee BC, Hwang WS, Lee CK.** Isolation and initial culture of porcine inner cell masses derived from in vitro-produced blastocysts. *Zygote* 2007; **15**: 55–63. [Medline] [CrossRef]
16. **Fujishiro SH, Nakano K, Mizukami Y, Azami T, Arai Y, Matsunari H, Ishino R, Nishimura T, Watanabe M, Abe T, Furukawa Y, Umeyama K, Yamanaka S, Ema M, Nagashima H, Hanazono Y.** Generation of naive-like porcine-induced pluripotent stem cells capable of contributing to embryonic and fetal development. *Stem Cells Dev* 2013; **22**: 473–482. [Medline] [CrossRef]
17. **Virag JA, Rolle ML, Reece J, Hardouin S, Feigl EO, Murry CE.** Fibroblast growth factor-2 regulates myocardial infarct repair: effects on cell proliferation, scar contraction, and ventricular function. *Am J Pathol* 2007; **171**: 1431–1440. [Medline] [CrossRef]
18. **Rasmussen MA.** Embryonic stem cells in the pig: characterization and differentiation into neural cells. *Depart Basic Ani Vet Univer Copen* 2012; 1–187.
19. **Williams DB, Carter CB.** The transmission electron microscope. Transmission Electron Microscopy: A Textbook for Materials Science. New York: Springer, 1996; 3–17.
20. **Bozzola JJ, Russell LD.** The transmission electron microscope. Electron Microscopy: Principles and Techniques for Biologists. Massachusetts: Jones and Bartlett publishers, 1999; 2: 148–201.
21. **Gonda MA, Aaronson SA, Ellmore N, Zeve VH, Nagashima K.** Ultrastructural studies of surface features of human normal and tumor cells in tissue culture by scanning and transmission electron microscopy. *J Natl Cancer Inst* 1976; **56**: 245–263. [Medline]
22. **Moise P, Sylvie R, Marie A, Michele K, Nicole T, Elisabeth D.** Enterocyte-like dif-

ferentiation and polarization of the human colon carcinoma cell line Caco-2 in culture. *Biol Cell* 1983; **47**: 323–330.
23. **Hara S, Terauchi K, Koike I.** Abundance of viruses in marine waters: assessment by epifluorescence and transmission electron microscopy. *Appl Environ Microbiol* 1991; **57**: 2731–2734. [Medline]
24. **Huang X, El-Sayed IH, Qian W, El-Sayed MA.** Cancer cell imaging and photothermal therapy in the near-infrared region by using gold nanorods. *J Am Chem Soc* 2006; **128**: 2115–2120. [Medline] [CrossRef]
25. **Baharvand H, Matthaei KI.** The ultrastructure of mouse embryonic stem cells. *Reprod Biomed Online* 2003; **7**: 330–335. [Medline] [CrossRef]
26. **Sathananthan H, Pera M, Trounson A.** The fine structure of human embryonic stem cells. *Reprod Biomed Online* 2002; **4**: 56–61. [Medline] [CrossRef]
27. **Alharbi S, Elsafadi M, Mobarak M, Alrwili A, Vishnubalaji R, Manikandan M.** Ultrastructural characteristics of three undifferentiated mouse embryonic stem cell lines and their differentiated three-dimensional derivatives: a comparative study. *Cell Rep* 2014; **16**: 151–165.
28. **Desbaillets I, Ziegler U, Groscurth P, Gassmann M.** Embryoid bodies: an in vitro model of mouse embryogenesis. *Exp Physiol* 2000; **85**: 645–651. [Medline] [CrossRef]
29. **Talbot NC, Garrett WM.** Ultrastructure of the embryonic stem cells of the 8-day pig blastocyst before and after in vitro manipulation: development of junctional apparatus and the lethal effects of PBS mediated cell-cell dissociation. *Anat Rec* 2001; **264**: 101–113. [Medline] [CrossRef]
30. **Kim E, Hwang SU, Yoo H, Yoon JD, Jeon Y, Kim H, Jeung EB, Lee CK, Hyun S-H.** Putative embryonic stem cells derived from porcine cloned blastocysts using induced pluripotent stem cells as donors. *Theriogenology* 2015., in press. [Medline] [CrossRef]
31. **Jeon Y, Kwak S-S, Cheong S-A, Seong YH, Hyun S-H.** Effect of trans-ε-viniferin on in vitro porcine oocyte maturation and subsequent developmental competence in preimplantation embryos. *J Vet Med Sci* 2013; **75**: 1277–1286. [Medline] [CrossRef]
32. **Kim E, Jeon Y, Kim DY, Lee E, Hyun S-H.** Antioxidative effect of carboxyethylgermanium sesquioxide (Ge-132) on IVM of porcine oocytes and subsequent embryonic development after parthenogenetic activation and IVF. *Theriogenology* 2015; **84**: 226–236. [Medline] [CrossRef]
33. **Kwak S-S, Cheong S-A, Jeon Y, Lee E, Choi K-C, Jeung E-B, Hyun SH.** The effects of resveratrol on porcine oocyte in vitro maturation and subsequent embryonic development after parthenogenetic activation and in vitro fertilization. *Theriogenology* 2012; **78**: 86–101. [Medline] [CrossRef]
34. **Jeon Y, Jeong SH, Biswas D, Jung EM, Jeung EB, Lee ES, Hyun SH.** Cleavage pattern and survivin expression in porcine embryos by somatic cell nuclear transfer. *Theriogenology* 2011; **76**: 1187–1196. [Medline] [CrossRef]
35. **Calarco PG, McLaren A.** Ultrastructural observations of preimplantation stages of the sheep. *J Embryol Exp Morphol* 1976; **36**: 609–622. [Medline]
36. **Hurst PR, Jefferies K, Eckstein P, Wheeler AG.** An ultrastructural study of preimplantation uterine embryos of the rhesus monkey. *J Anat* 1978; **126**: 209–220. [Medline]
37. **Mohr LR, Trounson AO.** Comparative ultrastructure of hatched human, mouse and bovine blastocysts. *J Reprod Fertil* 1982; **66**: 499–504. [Medline] [CrossRef]
38. **Scheer U, Hock R.** Structure and function of the nucleolus. *Curr Opin Cell Biol* 1999; **11**: 385–390. [Medline] [CrossRef]
39. **Olson MO, Dundr M, Szebeni A.** The nucleolus: an old factory with unexpected capabilities. *Trends Cell Biol* 2000; **10**: 189–196. [Medline] [CrossRef]
40. **Grewal SI, Moazed D.** Heterochromatin and epigenetic control of gene expression. *Science* 2003; **301**: 798–802. [Medline] [CrossRef]
41. **Nicolini C.** Chromatin structure: from nuclei to genes (review). *Antican Resear* 1982; **3**: 63–86.
42. **Van Blerkom J, Manes C, Daniel JC Jr.** Development of preimplantation rabbit embryos in vivo and in vitro. I. An ultrastructural comparison. *Dev Biol* 1973; **35**: 262–282. [Medline] [CrossRef]
43. **Sathananthan H, Bongso A, Ng S-C, Ho J, Mok H, Ratnam S.** Ultrastructure of preimplantation human embryos co-cultured with human ampullary cells. *Hum Reprod* 1990; **5**: 309–318. [Medline]
44. **Barr FA, Warren G.** Disassembly and reassembly of the Golgi apparatus. *Semin Cell Dev Biol* 1996; **7**: 505–510. [CrossRef]
45. **Barr FA, Short B.** Golgins in the structure and dynamics of the Golgi apparatus. *Curr Opin Cell Biol* 2003; **15**: 405–413. [Medline] [CrossRef]
46. **Wang J, Luo J, Zhang X.** [From endoplasmic reticulum to Golgi apparatus: a secretory pathway controlled by signal molecules]. *Zhejiang da xue xue bao Yi xue ban. J Zheji Univer Med Sci* 2013; **42**: 427–472.
47. **Plante L, King WA.** Light and electron microscopic analysis of bovine embryos derived by in vitro and in vivo fertilization. *J Assist Reprod Genet* 1994; **11**: 515–529. [Medline] [CrossRef]
48. **Enders A.** The fine structure of the blastocyst. *USAID* 1971:71–94.
49. **Aderem A, Underhill DM.** Mechanisms of phagocytosis in macrophages. *Annu Rev Immunol* 1999; **17**: 593–623. [Medline] [CrossRef]
50. **Desjardins M.** ER-mediated phagocytosis: a new membrane for new functions. *Nat Rev Immunol* 2003; **3**: 280–291. [Medline] [CrossRef]
51. **Baba M, Takeshige K, Baba N, Ohsumi Y.** Ultrastructural analysis of the autophagic process in yeast: detection of autophagosomes and their characterization. *J Cell Biol* 1994; **124**: 903–913. [Medline] [CrossRef]
52. **Kishi-Itakura C, Koyama-Honda I, Itakura E, Mizushima N.** Ultrastructural analysis of autophagosome organization using mammalian autophagy-deficient cells. *J Cell Sci* 2014; **127**: 4089–4102. [Medline] [CrossRef]
53. **de Paz P, Sánchez AJ, De la Fuente J, Chamorro CA, Alvarez M, Anel E, Anel L.** Ultrastructural and cytochemical comparison between calf and cow oocytes. *Theriogenology* 2001; **55**: 1107–1116. [Medline] [CrossRef]
54. **Picard M, Taivassalo T, Gouspillou G, Hepple RT.** Mitochondria: isolation, structure and function. *J Physiol* 2011; **589**: 4413–4421. [Medline] [CrossRef]
55. **Stern S, Biggers JD, Anderson E.** Mitochondria and early development of the mouse. *J Exp Zool* 1971; **176**: 179–191. [Medline] [CrossRef]
56. **Heath-Engel HM, Shore GC.** Mitochondrial membrane dynamics, cristae remodelling and apoptosis. *Biochim Biophys Acta* 2006; **1763**: 549–560. [Medline] [CrossRef]
57. **Picard M, Taivassalo T, Ritchie D, Wright KJ, Thomas MM, Romestaing C, Hepple RT.** Mitochondrial structure and function are disrupted by standard isolation methods. *PLoS ONE* 2011; **6**: e18317. [Medline] [CrossRef]
58. **Duchen MR.** Mitochondria in health and disease: perspectives on a new mitochondrial biology. *Mol Aspects Med* 2004; **25**: 365–451. [Medline] [CrossRef]
59. **Johannsen DL, Ravussin E.** The role of mitochondria in health and disease. *Curr Opin Pharmacol* 2009; **9**: 780–786. [Medline] [CrossRef]
60. **Russell LD, Peterson RN.** Sertoli cell junctions: morphological and functional correlates. *Int Rev Cytol* 1985; **94**: 177–211. [Medline] [CrossRef]
61. **Dejana E.** Endothelial cell-cell junctions: happy together. *Nat Rev Mol Cell Biol* 2004; **5**: 261–270. [Medline] [CrossRef]
62. **Panigel M, Kraemer D, Kalter S, Smith G, Heberling R.** Ultrastructure of cleavage stages and preimplantation embryos of the baboon. *Anat Embry* 1974; **147**: 45–62.
63. **Mohr LR, Trounson AO.** Structural changes associated with freezing of bovine embryos. *Biol Reprod* 1981; **25**: 1009–1025. [Medline] [CrossRef]
64. **Dale B, Gualtieri R, Talevi R, Tosti E, Santella L, Elder K.** Intercellular communication in the early human embryo. *Mol Reprod Dev* 1991; **29**: 22–28. [Medline] [CrossRef]
65. **Zakeri Z, Lockshin RA.** Cell death during development. *J Immunol Methods* 2002; **265**: 3–20. [Medline] [CrossRef]
66. **Ferri KF, Kroemer G.** Organelle-specific initiation of cell death pathways. *Nat Cell Biol* 2001; **3**: E255–E263. [Medline] [CrossRef]
67. **Bursch W.** The autophagosomal-lysosomal compartment in programmed cell death. *Cell Death Differ* 2001; **8**: 569–581. [Medline] [CrossRef]
68. **Jacobson MD, Weil M, Raff MC.** Programmed cell death in animal development. *Cell* 1997; **88**: 347–354. [Medline] [CrossRef]
69. **Kroemer G, Reed JC.** Mitochondrial control of cell death. *Nat Med* 2000; **6**: 513–519. [Medline] [CrossRef]
70. **Stroband HW, Taverne N, vd Bogaard M.** The pig blastocyst: its ultrastructure and the uptake of protein macromolecules. *Cell Tissue Res* 1984; **235**: 347–356. [Medline] [CrossRef]
71. **Hyttel P, Laurincik J, Rosenkranz C, Rath D, Niemann H, Ochs RL, Schellander K.** Nucleolar proteins and ultrastructure in preimplantation porcine embryos developed in vivo. *Biol Reprod* 2000; **63**: 1848–1856. [Medline] [CrossRef]